Initial results of the Netlander imaging ground-penetrating radaroperated on the Antarctic Ice Shelf

Jean-Jacques Berthelier, S. Bonaimé, Valérie Ciarletti, R. Clairquin, F. Dolon, Alice Le Gall, D. Nevejans, Richard Ney, Alain Reineix

Initial results of the Netlander imaging ground-penetrating radar operated on the Antarctic Ice Shelf

J. J. Berthelier,[1] S. Bonaimé,[1,2] V. Ciarletti,[1] R. Clairquin,[3] F. Dolon,[1] A. Le Gall,[1] D. Nevejans,[3] R. Ney,[1] and A. Reineix[4]

Received 26 July 2005; revised 16 September 2005; accepted 5 October 2005; published 18 November 2005.

[1] The objective of the Netlander mission was to land 4 small geophysical stations on the surface of Mars to study the deep interior, subsurface, surface and atmosphere of the planet. Included in the payload was a ground penetrating radar (GPR) designed to retrieve not only the distance but also the direction of the reflectors, thus providing a simplified 3D imaging of the subsurface. In this paper we report initial results obtained during the RANETA campaign on the Antarctic ice shelf. Data from two soundings of the ice-bed rock interface are analyzed, demonstrating the capability of the radar to disentangle echoes from different reflecting facets of the bed rock. **Citation:** Berthelier, J. J., S. Bonaimé, V. Ciarletti, R. Clairquin, F. Dolon, A. Le Gall, D. Nevejans, R. Ney, and A. Reineix (2005), Initial results of the Netlander imaging ground-penetrating radar operated on the Antarctic Ice Shelf, *Geophys. Res. Lett.*, *32*, L22305, doi:10.1029/2005GL024203.

1. Description of the Experiment

[2] The Netlander GPR has been described in previous papers [*Berthelier et al.*, 2000; 2003] and the instrument principle will be briefly recalled here. The main objective of the experiment was to achieve long range soundings to possibly access to liquid water reservoirs in the Martian underground. According to Martian geological models [*Fanale et al.*, 1986; *Clifford*, 1993], the depth of transition from ground ice to liquid water is expected to range from 1 to 3 kilometers at low latitudes. The objective set to the GPR was thus to reach a depth of about 2 kilometers and a low frequency range of operation, from 2 to 4 MHz, was selected. Numerical simulations have been conducted to model the radar operation [*Ciarletti et al.*, 2003] using geological models of the subsurface based in part on measured electromagnetic properties of terrestrial analogues of Martian materials [*Heggy et al.*, 2003]. The most challenging problem faced by the Netlander GPR was to operate from a fixed lander which cannot be moved over the surface as is ordinarily done to retrieve 2D or 3D sub-surface profiles [e.g. *Habashy and Mitra*, 1987]. An innovative concept was thus proposed to determine simultaneously the distance and the direction of the underground reflectors. In the case of a rather homogeneous medium such as the Antarctic ice cap, the direction of a reflector is given by the direction of propagation of reflected waves and this latter can be retrieved from the analysis of the electric and magnetic components of the waves [*Berthelier et al.*, 2000]. To this aim, the RANETA radar is equipped with two orthogonal dipolar electric antennas laid on the surface and defining the horizontal Ox and Oy axis (with Oz as the ascending vertical), and with a receiving magnetic antenna that is successively oriented along Ox, Oy and Oz during a sequence of measurement. Each electric antenna consists of two opposite broad band resistively damped quarter-wave monopoles [*Wu and King*, 1965]. The magnetic antenna is a search coil antenna. The radar controller is built around a single FPGA which determines the sequence of operation, generates the transmitted signal through a Direct Digital Synthesis (DDS) embedded code and performs the sampling and A/D conversion of the received signals. The analog electronics includes the clock generation from an ultra stable OCXO, the transmitter filters and amplifiers, the variable gain receiver and various switches. Thanks to the fully digital signal generation and the ultra low jitter of the sampling clock, the received signals are sampled at phase lags that are perfectly fixed with respect to the transmitted signal and this allows one to perform a large number of coherent additions to increase the radar sensitivity. The transmitter amplifier delivers a nominal power of 10 W but, in the present prototype, coupling losses and antenna efficiency reduce the effective transmitted power to $\sim$0.1 W. The sensitivity of the electric and magnetic channels is respectively $\sim$0.2 nV.m^{-1}.Hz$^{-1/2}$ and $\sim$5.10^{-15} T.Hz$^{-1/2}$. In order to reduce the level of electromagnetic interferences, bi-phasing is used during a transmission sequence by alternating waveforms of opposite polarities and performing correspondingly additions or subtractions during the coherent addition process. For the electric channels, co-polar and cross-polar measurements were made using the two orthogonal antennas.

2. Observations

[3] During the RANETA campaign, 8 soundings were performed in the vicinity of the French-Italian Cap Prudhomme station (139.90 E, 66.68 S) at distances from the coast from $\sim$5 km to $\sim$45 km corresponding to altitudes of $\sim$285 m to $\sim$1100 m above sea level. Gneiss is the dominant material in the bedrock. A sketch of the radar,

[1]Centre d'études des Environnements Terrestre et Planétaire, Institut Pierre-Simon Laplace, Saint-Maur, France.
[2]Now at Institut de Physique du Globe de Paris, University Paris 7, Paris, France.
[3]Belgisch Instituut voor Ruimte-Aëronomie, Institut d'Aéronomie Spatiale de Belgique, Brussels, Belgium.
[4]Institut de Recherche en Communications Optiques et Microondes, Université de Limoges, Limoges, France.

0094-8276/05/2005GL024203

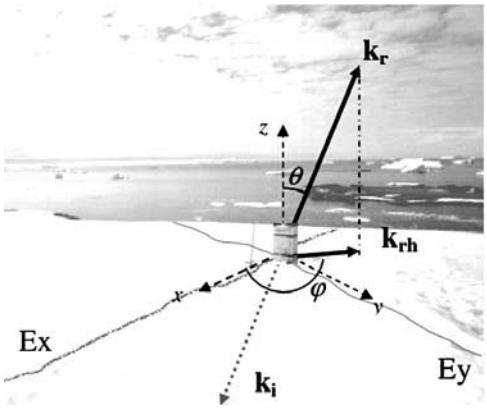

Figure 1. Schematic view of the radar, its electric antennas and of the frame of reference.

its antennas and the frame of reference that will be used in the following is given in Figure 1.

2.1. Antenna Impedance Measurements

[4] Reflected waves propagating backward to the surface are refracted when exiting into the atmosphere. The electromagnetic parameters of the shallow underground have thus to be known to properly determine the propagation vector in the subsurface. The impedance of the electric antennas depends on the electric permittivity ε and conductivity σ of the sub-surface, averaged over a depth which is commensurate with the length of the antenna. The numerical FDTD model of the radar [*Ciarletti et al.*, 2003] was used to compute the complex antenna impedance as a function of frequency. The modeled real and imaginary terms of the impedance vary rapidly as a function of frequency below ~2 MHz but very slowly above that frequency [*Bauchet*, 2004]. Detailed comparisons between the model results and measurements over a soil of known electromagnetic show an excellent agreement with an accuracy of 5 to 10% on fitted values of ε and σ. During the RANETA campaign, a dedicated mode of operation of the radar was used to measure the electric antenna impedance between 0.4 and 8 MHz, a range which encompasses the largest part of the frequency spectrum of the transmitted wave pulses at centre frequencies from 2 to 4 MHz. Values of 3.4 and 2.5 10^{-5} S were found for ε and σ respectively, in good agreement with published values for ice under similar temperature conditions [*Fujita et al.*, 2000].

2.2. Radar Soundings

[5] Raw waveforms of the 2 electric (upper curves) and 3 magnetic (lower curves) components of reflected waves are presented in Figures 2 (left) and 3 (left) for two soundings performed respectively at ~20 km (January 29, case 1) and ~30 km (February 1st, case 2) from the coast. A 1 μs long, Gaussian shaped pulse with a 4 MHz centre frequency was transmitted through the Ex antenna. In order to improve the S/N ratio of these measurements, in particular of the *Hz* or *Hx* magnetic components that were subject to interferences, data were processed through a numerical Wiener filter and filtered data are shown in Figures 2 (right) and 3 (right). In case 1, the Ex waveform distinctly shows two echoes that originate from reflection on the ice-bedrock interface at ~6.1 and ~8.3 μs respectively. Similar echoes are also observed on the Ey antenna signal but with a much weaker level and with a waveform more complex and extended in time. The Ey antenna being orthogonal to the transmitting Ex antenna, the smaller level of the returning signal indicates that the interface is rather smooth at the ~100 m scale of the transmitted wavelengths. The two main echoes observed on Ex are also observed on the magnetic antennas. In case 2, a single signal is observed on the Ex antenna at ~10 μs with no distinct delayed signal. The signal on the Ey antenna is much weaker and extended in time for the same reasons as in case 1. Similarly a single signal is detected on the magnetic antennas although slightly more extended in time than on the Ex antenna.

3. Data Analysis and Results

[6] Before processing the data to retrieve the direction of the propagation vector, magnetic data have to be corrected from two main parasitic effects (i) the existence of a magnetic field induced by the current flowing in the electric antennas when excited by the electric field of the reflected wave, and (ii) the imperfect decoupling of the magnetic antenna with respect to components perpendicular to its axis. The far field limit of the radar being about 150 meters [*Berthelier et al.*, 2000], waves incident on the bedrock can be considered as locally plane waves with electric and magnetic components **Ei** and **Hi** perpendicular to the propagation direction defined by its unit vector **ki**. Since the radar is mono-static and measures reflected waves at the location of the transmitter, the detected waves arise from the reflection of the incident waves on a facet of the bedrock that is perpendicular to **ki**. The **Er** and **Hr** components of the reflected waves are perpendicular to their propagation direction defined by its unit vector **kr**, opposite to **ki**, and a straightforward method to retrieve the propagation direction

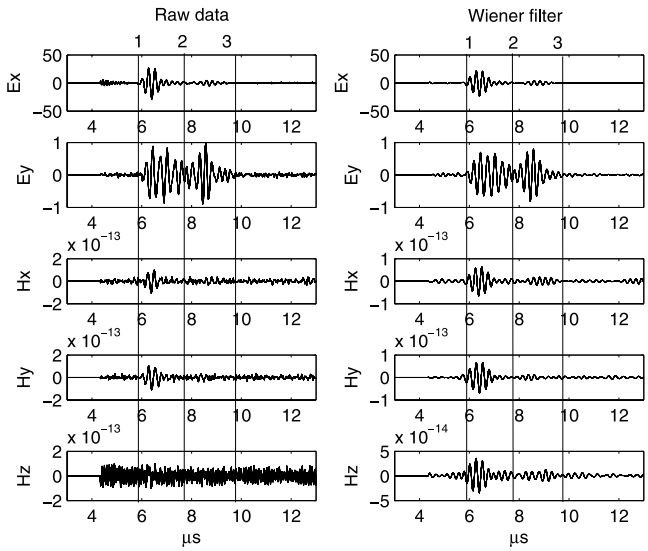

Figure 2. January 29th, 2004 sounding, (left) raw data, (right) Wiener filtered data. The unit along the X axis is the delay time in μs, units along the Y axis are in mV at the output of the electric receivers and in Teslas for the magnetic channels.

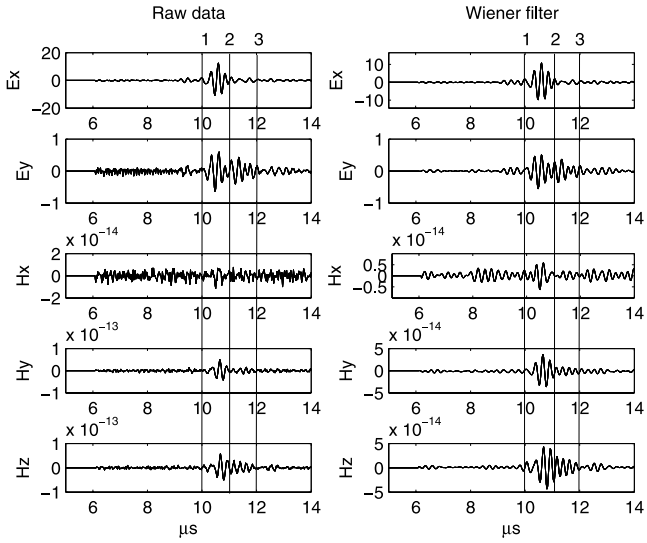

Figure 3. February 1st, 2004 sounding, (left) raw data, (right) Wiener filtered data, same units as in Figure 2.

should thus be to compute **Er**^**Hr**. E_{rz} the only component of the returning wave which is not directly measured is needed but can be obtained by expressing that **Er** and **Hr** are perpendicular, hence

$$E_{rz} = -\frac{\left(H_{rx}E_{rx} + H_{ry}E_{ry}\right)}{H_{rz}} \quad (1)$$

However, since reflected waves are in general propagating at relatively small angles from the vertical direction, their electric and magnetic fields vectors remain close to the horizontal plane and H_{rz} is small. This entails too large errors in the computed value of E_{rz} and, in practice, often precludes one to use this simple method. We have thus derived a second method which is based on the use of the magnetic components alone. Its principle can be briefly described as follows. Let **x**, **y**, **z** be the unit vectors of the Oxyz reference frame and θ and φ the angles defining the direction of the unit vector **kr** with θ = (**z**, **kr**) and φ = (**x**, $\mathbf{kr_h}$) where $\mathbf{kr_h}$ is the horizontal component of **kr** (see Figure 1). Let **X**, **Y**, **Z** be the unit vectors in the plane of the reflecting facet with **X** in the (**z**, **kr**) plane. Let $\mathbf{H_0}$ be the magnetic field of the transmitted wave at the far field boundary. $\mathbf{H_0}$ is parallel to the (**X**,**Y**) plane and its components H_{oX} and H_{oY} along X and Y respectively can be written as H_o cos α and H_o sin α. Normalizing the measured components of the magnetic field H_x, H_y and H_z with respect to the amplitude of the measured magnetic field H, $h_x = H_x/H$ etc…, a straightforward calculation leads to the following relations:

$$h_x(t) = (\cos\alpha\cos\theta\cos\varphi - \sin\alpha\sin\varphi) f(t, H_o/H, d, n_1, n_2) \quad (2)$$

$$h_y(t) = (\cos\alpha\cos\theta\sin\varphi + \sin\alpha\cos\varphi) f(t, H_o/H, d, n_1, n_2) \quad (3)$$

$$h_z(t) = (\cos\alpha\sin\theta) f(t, H_o/H, d, n_1, n_2) \quad (4)$$

Since we are only interested in determining θ and φ and the distance d, the attenuation of the reflected waves through geometrical spreading, propagation losses and reflection included in $f(t, H_o/H, d, n_1, n_2)$ is simply taken into account by normalizing the amplitude of the detected signals to the reference waveform at the time of transmission. The function f also includes the shift in time, equal to the propagation time τ of the reflected wave. τ is determined by correlating the received electric field waveform (due to its very good S/N ratio) with the reference waveform. To a good approximation, $\tau = d/v_1(\omega)$ where $v_1(\omega) = c/n_1(\omega)$ is the propagation velocity at the centre frequency of the transmitted pulse. Due to the rather good homogeneity of the ice from the surface to the bedrock, we assume that $n_1(\omega)$ is constant along the propagation path and equal to the value deduced from the antenna impedance measurements. From τ the value of d can therefore be obtained. We are thus left with a set of 3 non linear equations (2), (3), (4) with 3 unknown angles θ, φ, α that is solved using an iteration technique. As mentioned above, one has to take into account the refraction of the wave at the exit from the ice to derive the propagation angles θ* and φ* in the subsurface from the computed values of θ and φ.

[7] For the two examples shown in Figures 2 and 3 the results are the following:

- case 1 reflecting facet 1: $\theta_1^* = 17°$, $\varphi_1^* = 155°$ and d_1 = 509 m
  reflecting facet 2: $\theta_2^* = 39°$, $\varphi_2^* = 181°$ and d_2 = 542 m
- case 2 reflecting facet: $\theta_1^* = 29°$, $\varphi_1^* = 171°$ and d_1 = 760 m

Estimated uncertainties are typically 10° to 15° on θ and φ and ∼60 meters on d. The main source of errors in the determination of the direction of the reflectors is linked to the parasitic effects on magnetic measurements. An improved correction algorithm is presently being developed which significantly reduces these uncertainties.

[8] The retrieved φ angles are close to 180°. This result is in agreement with the observed strong maximum of the received electric signal along the (transmitting) Ex antenna: waves detected by the radar propagate close to the vertical Oxz plane containing the Ex antenna. No detailed topographic information on the bedrock is available over the area where the soundings have been performed but, within 20 to 30 kilometers from the coast it is thought that the average level of the bedrock stays quite close to the sea level. Taking into account the values of θ*, the retrieved distances compare reasonably well with the altitudes of the two sites, respectively 413 m and 618 m. The main echoes correspond to propagation θ* angles of about 25° ± 5° and the second echo in case 1 corresponds to a propagation significantly off vertical. Two reasons can be advocated to explain these observations. First, the radiation pattern of interfacial dipole antennas over a soil with n ∼ 3.3 shows a secondary maximum around ∼20° to 25° off vertical in the vertical plane containing the antenna [*Engheta et al.*, 1982], and the sensitivity of the radar is enhanced in this angular range. In addition, close to the region where the RANETA campaign took place, the topography of the coast and islands is very much irregular and this is probably true also for the bedrock under the ice shelf.

In such conditions, it is not astonishing to observe oblique echoes.

4. Conclusion

[9] We have presented two of the soundings performed with a prototype of the Netlander GPR on the Antarctic ice shelf over an ice thickness from ~500 m to 750 m. In one case, the analysis performed on the measured 3 magnetic components of the reflected waves has shown that these waves were reflected from two distinct facets of the bedrock and the location of these facets were determined. This initial result, in good agreement with previous simulation results, shows that the specific concept of the radar allows one to disentangle echoes from various reflecting facets of an interface. An improved method of analysis is presently being developed to make full use of the imaging capabilities of the radar and obtain a comprehensive description of the bedrock topography and roughness. If the imaging concept is necessary to interpret soundings performed from a single fixed location, such a technique can also significantly improve the performances of ground penetrating radars operated in a standard mode on a network of positions to retrieve the 2D or 3D structure of the underground.

[10] **Acknowledgment.** We thank IPEV (Institut Paul-Emile Victor) who was in charge of the organization of the RANETA campaign and CNES for funding the development of the radar under grants 793/CNES/99/7947 and 737/CNES/00/8261.

References

Bauchet, G. (2004), Etude théorique et validation expérimentale de l'analyse électromagnétique d'un radar destiné au sondage du sous-sol martien, these, Univ. de Limoges, Limoges, France.

Berthelier, J. J., et al. (2000), The GPR experiment on Netlander, *Planet. Space Sci.*, *48*, 1161–1180.

Berthelier, J.-J., et al. (2003), GPR, a ground-penetrating radar for the Netlander mission, *J. Geophys. Res.*, *108*(E4), 8027, doi:10.1029/2002JE001866.

Ciarletti, V., B. Martinat, A. Reineix, J. J. Berthelier, and R. Ney (2003), Numerical simulation of the operation of the GPR experiment on Netlander, *J. Geophys. Res.*, *108*(E4), 8028, doi:10.1029/2002JE001867.

Clifford, S. M. (1993), A model for the hydrologic and climatic behavior of water on Mars, *J. Geophys. Res.*, *98*(E6), 10,973–11,016.

Engheta, N., C. H. Papas, and C. Elachi (1982), Radiation patterns of interfacial dipole antennas, *Radio Sci.*, *17*, 1557–1566.

Fanale, F. P., J. R. Salvail, A. P. Zent, and S. E. Postawko (1986), Global distribution and migration of subsurface ice on Mars, *Icarus*, *67*, 1–18.

Fujita, S., T. Matsuoka, T. Ishida, K. Matsuoka, and S. Mae (2000), A summary of the complex dielectric permittivity of ice in the megahertz range and its applications for radar sounding of polar ice sheets, in *Physics of Ice Core Records*, pp. 185–212, Hokkaido Univ. Press, Sapporo, Japan.

Habashy, T., and R. Mitra (1987), On some inverse methods in electromagnetics, *J. Electromagn. Waves Appl.*, *1*(1), 25–58.

Heggy, E., P. Paillou, F. Costard, N. Mangold, G. Ruffie, F. Demontoux, G. Grandjean, and J. M. Malézieux (2003), Local geoelectrical models of the Martian subsurface for shallow groundwater detection using sounding radars, *J. Geophys. Res.*, *108*(E4), 8030, doi:10.1029/2002JE001871.

Wu, T. T., and R. W. P. King (1965), The cylindrical antenna with non-reflecting resistive loading, *IEEE Trans. Antennas Propag.*, *13*(3), 369–373.

J. J. Berthelier, V. Ciarletti, F. Dolon, A. Le Gall, and R. Ney, CETP, IPSL, 4 avenue de Neptune, F-94100 Saint-Maur, France. (berthelier@cept.ipsl.fr)

S. Bonaimé, IPGP, University Paris 7, 4, place Jussieu, case 89, F-75252 Paris, France.

R. Clairquin and D. Nevejans, BIRA, IASB, Ringlaan 3, B-1180 Bruxelles, Belgium.

A. Reineix, IRCOM, Université de Limoges, 123, avenue Albert Thomas, F-87060 Limoges, France.